

P. Samyn

e-mail: Pieter.Samyn@UGent.be

W. Van Paepegem

Ghent University,
Laboratory Soete,
Department Mechanical Construction and
Production,
St. Pietersnieuwstraat 41,
B-9000 Gent,
Belgium

J. S. Leendertz

Ministry of Transport,
Public Works and Water Management,
Directorate-General,
Herman Gorterhove 4,
NL-2700 AB Zoetermeer,
The Netherlands

A. Gerber

University of Stuttgart,
Staatliche Materialprüfungsanstalt,
G-70550 Stuttgart (Vaihingen),
Germany

L. Van Schepdael

SOLICO B.V.,
Solutions in Composites,
Everdenberg 97,
NL-4902 TT Oosterhout,
The Netherlands

J. Degrieck

P. De Baets

Ghent University,
Laboratory Soete,
Department Mechanical Construction and
Production,
St. Pietersnieuwstraat 41,
B-9000 Gent,
Belgium

Large-Scale Evaluation of Constrained Bearing Elements Made of Thermosetting Polyester Resin and Polyester Fabric Reinforcement

Polymer composites are increasingly used as sliding materials for high-loaded bearings, however, their tribological characteristics are most commonly determined from small-scale laboratory tests. The static strength and dynamic coefficients of friction for polyester/polyester composite elements are presently studied on large-scale test equipment for determination of its bearing capacity and failure mechanisms under overload conditions. Original test samples have a diameter of 250 mm and thickness of 40 mm, corresponding to the practical implementation in the sliding surfaces of a ball-joint, and are tested at various scales for simulation of edge effects and repeatability of test results. Static tests reveal complete elastic recovery after loading to 120 MPa, plastic deformation after loading at 150 MPa and overload at 200 MPa. This makes present composite favorable for use under high loads, compared to, e.g., glass-fibre reinforced materials. Sliding tests indicate stick-slip for pure bulk composites and more stable sliding when PTFE lubricants are added. Dynamic overload occurs above 120 MPa due to an expansion of the nonconstrained top surface. A molybdenum-disulphide coating on the steel counterface is an effective lubricant for lower dynamic friction, as it favorably impregnates the composite sliding surface, while it is not effective at high loads as the coating is removed after sliding and high initial static friction is observed. Also a zinc phosphate thermoplastic coating cannot be applied to the counterface as it adheres strongly to the composite surface with consequently high initial friction and coating wear. Most stable sliding is observed against steel counterfaces, with progressive formation of a lubricating transfer film at higher loads due to exposure of PTFE lubricant. Composite wear mechanisms are mainly governed by thermal degradation of the thermosetting matrix (max. 162°C) with shear and particle detachment by the brittle nature of polyester rather than plastic deformation. The formation of a sliding film protects against fiber failure up to 150 MPa, while overload results in interlaminar shear, debonding, and ductile fiber pull-out. [DOI: 10.1115/1.2345413]

Keywords: ball-joint, composite, large-scale, strength, friction, wear mechanisms

1 Introduction

Polymers and polymer-based systems are increasingly used as constructional elements due to availability within a wide range of material properties, ease of manufacturing, good strength, and light weight. Besides original statically loaded applications [1], they are also effective in situations of sliding contact wear [2]. Polymers are preferred in recent years over metal-based counterparts in view of their self-lubricating ability and low friction [3], although their load sustaining capacity is often limited. The introduction of fiber reinforcements leads to higher strength but sig-

nificantly alters the tribological characteristics. For example, the inclusion of short glass fibers within a polyetherimide matrix improves the wear performance but deteriorates the friction behavior; it proved to be extremely good in adhesion and fretting wear modes but very poor in abrasive and erosive wear [4]. Also the presence of short glass fibers in polyamide 66 enhances the mechanical properties but it increases friction and wear rates gradually with higher fiber percentage [5]. Epoxy resins reinforced with high-strength glass fibers are frequently studied [6,7], although Jacobs et al. [8] noticed no significant improvement in wear resistance compared to neat epoxy. It is known that the glass fibers have relatively higher coefficient of friction than the epoxy matrix and loss of debris increases the abrasive wear damaging the counterpart.

Thermosetting polyesters are commonly used as matrix mate-

Contributed by the Tribology Division of ASME for publication in the JOURNAL OF TRIBOLOGY. Manuscript received February 16, 2006; final manuscript received June 14, 2006. Review conducted by Michael Lovell.

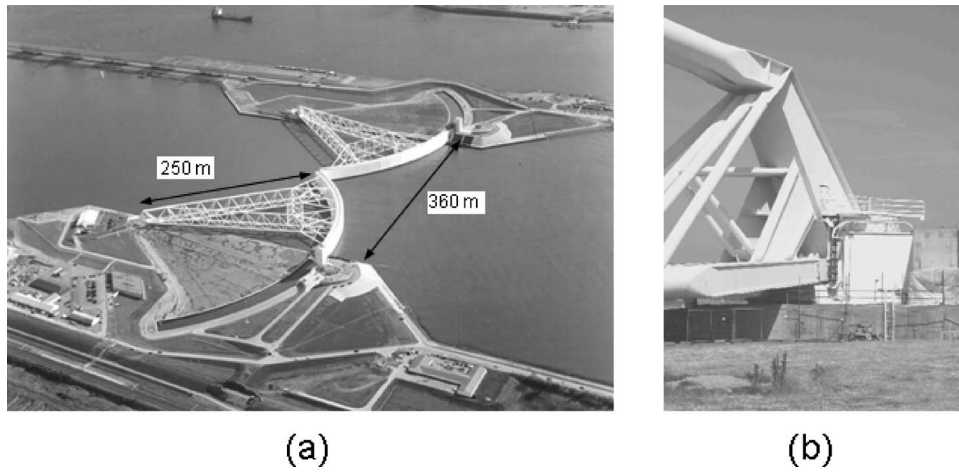


Fig. 1 Use of a high-loaded ball-joint in the Maeslant storm surge barrier, near Rotterdam (NL), (a) general view on the barrier closing the Nieuwe Waterweg with hemispherical gates connected by steel trusses to a ball-joint in the abutments, (b) detail of the connection between steel trusses and the ball-joint in a climate controlled room

rial, particularly with either oxide compounds [9] or glass fiber reinforcements [10–13]. A recent investigation [14] showed that glass fiber reinforced polyester composites give higher wear resistance than the plain polyester. In case of laminated glass fiber composites, the wear properties are strongly influenced by the laminate orientation [15]. In another work [16], the lowest wear and friction coefficients are obtained for fibers oriented normal to the sliding surface. Polyesters with chopped strand mat glass fibers indicate that the fiber direction inducing lowest wear rates also depends on the sliding speed. Sometimes three-body abrasive wear was noticed [17]. As polyester is an economic material that has high chemical resistance, good dimensional stability and low moisture absorption it remains a favorable matrix material. To the authors' knowledge, very few information is available on the tribological performance of a thermosetting polyester matrix reinforced with thermoplastic polyester fibers. From mechanical point of view they possess extremely good elasticity to be considered for functioning in heavy duty bearings.

Numerous sliding tests on polymer composites are done on small-scale bloc-on-ring tests [18] or pin-on-disc tests with either a stationary composite pin [19] or rotating composite disc [20], identifying different wear mechanisms such as fiber-matrix debonding, fiber cracking, fiber pull out, etc. As tribological performance is strongly related to the practical working conditions, large-scale tests become more effective in relation to practical bearing design combining both static and dynamic properties. Mainly when used at high contact pressures, the visco-elastic properties of composites and stress concentrations near the edges of the samples should be effectively simulated. Composite sliding elements are not only used as tribological elements, but integrated within a bearing they form a functional part. A major problem in this respect is the dimensional stability of bearing elements during loading and unloading as high deformation can cause failure of the entire construction through loss of clearance rather than through wear.

Present investigation found its origin in the design of sliding surfaces for a ball-joint, used in the Maeslant storm surge barrier (Fig. 1(a)). The barrier has of two hemispherical gates that are connected by steel trusses to a ball-joint (Fig. 1(b)) for multi-axial rotation of the gates from the parking docks into the water (horizontal rotation) and sinking to the riverbed (vertical rotation). The ball-joint detailed in Fig. 2 has two segmented ball scales transmitting the horizontal forces directly to the front and back chairs and the vertical forces to a bearing element with the shape of a

ring. It has a diameter of 10 m and a weight of 680 tons, transmitting a total resultant force of $350 \cdot 10^6$ N under full hydraulic head [21].

The convex and concave surfaces were originally covered with one 10 μ m thick layer that is a mixture of MoS_2 and PTFE resin, in order to obtain low friction. For running-in purposes an additional layer of PTFE-spray was applied to overcome static friction. After several sliding steps the coating was removed from the contact zone and cold welding spots were observed through adhesive steel/steel contact. A modified design was studied, containing an elastic bearing layer between both surfaces. Two alternatives were, therefore, investigated:

- A first design of "free" composite pads bolted on the concave surfaces was considered (Fig. 3(a)). Forces will

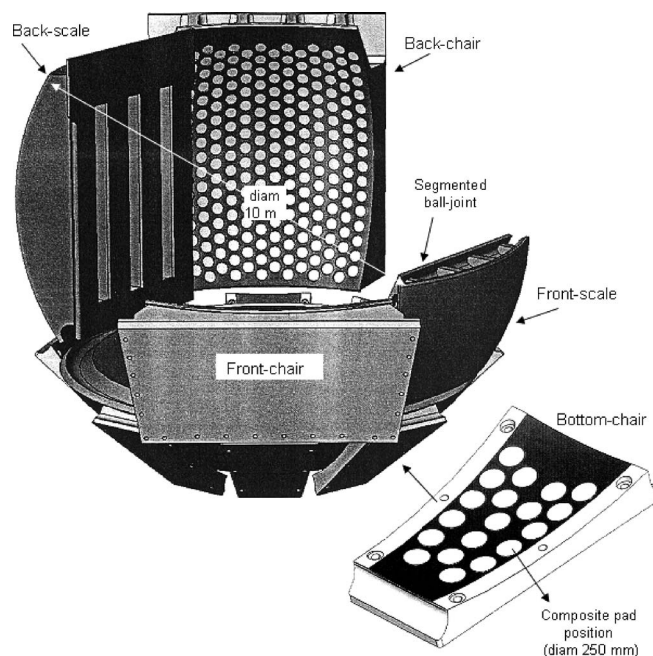


Fig. 2 Detail of the inner structure of the ball-joint for application of composite bearing elements

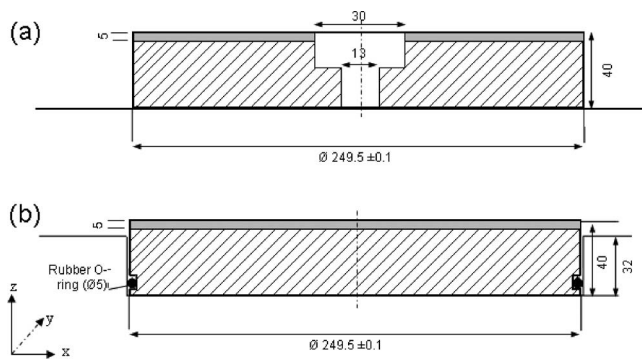


Fig. 3 Detail of a polyester/polyester composite pad with nominal diameter 250 mm and thickness 40 mm as sliding element in the ball-joint (grey zone indicates 5 mm internal lubricated top layer of polyester/polyester B) (a) free composite pad, (b) constrained composite pad

then be transferred from the convex onto the concave surfaces and foundations of the structure through friction between the composite bottom surface and the concave steel surface. The friction coefficient of the top surface of the composite pad in contact with the convex cast steel should, therefore, be lower than the friction coefficient of the bottom surface in contact with the concave cast iron, which is possible by introducing a solid lubricant on the top sliding surface and increasing the roughness of the bottom sliding surface. A polymer screw in the center of the pad is used for axial fixation, while permanent positioning of the pads is ensured by high friction between the composite pad and the concave surface.

- A second design consists of constrained composite pads, incorporated into 468 holes machined on the concave back, bottom and front surfaces of the ball-joint (Fig. 3(b)). The pad should have a nominal diameter of 249.50 mm and a thickness of 40 mm while the machined holes have a diameter of 250 and 32 mm depth. It means that the polymer has a free surface of 8 mm above the concave chair structures in contact with the convex steel counterface.

The local stiffness and friction of a single composite bearing element is an important issue for proper functioning of the ball-joint, as it influences the roll and slip motions of the convex into the concave surfaces [22]. The static and dynamic loading capacity should be experimentally verified by a large-scale test set-up simulating the practical boundary conditions as close as possible. The influence of different counterface types on friction and wear will be investigated, applying either low carbon steel St 32-7 or a MoS₂ thin film or a zinc phosphate primer coating, in combination with creep under various preloads and geometrical scales, giving additional insight into the reproducibility of the test results. The wear of composite pads and counterfaces was evaluated by microscopy. An international test program was set up by the Dutch Ministry of Transport, Water Management and Public Works, Civil Engineering Division (Nederlandse Rijkswaterstaat), Ghent

University (Laboratory Soete), Stuttgart University (Materialprüfungsanstalt) and Solico BV (Solutions in Composites).

2 Experimental

2.1 Test Material. Composite pads consist of woven polyester fabrics (90 deg) impregnated with a thermosetting polyester resin. The polyester/polyester A type is a pure bulk composite, the polyester/polyester B type has 10 to 15 wt % PTFE lubricants homogeneously dispersed into the polyester matrix over a depth of about 5 mm beneath the sliding surface (Fig. 3). The mechanical properties of polyester/polyester A and B are given in Table 1. It is thermally stable between -40°C and 130°C in dry environments. A reference pv-limit of 1.6 MPa.m/s under dry sliding is indicated in manufacturer's reports [23], based on small-scale tests. In this investigation, the A-grade will be evaluated only under large-scale dynamic sliding. The B-grade will be evaluated under large-scale static loading and dynamic sliding.

The polyester/polyester composite is until now mainly used in cylindrical bearings, running at 0.5 m/s sliding speed and 15 MPa contact pressure against stainless steel counterfaces. Pin-on-disc small-scale tests indicate a coefficient of friction 0.20 (polyester/polyester A) to 0.15 (polyester/polyester B) at high velocity and low contact pressures [23]. Although the material has potential to be used at extremely high loads, little relevant literature is available about its sliding characteristics and wear mechanisms, partly due to the lack of appropriate testing facilities. The independent elastic properties were determined from preliminary tensile tests, compression tests and short beam shear tests as follows [24]: $E_{11}=2.36$ GPa, $E_{22}=2.19$ GPa, $\nu_{12}=0.30-0.35$, $\nu_{23}=0.45-0.50$ (experimental), and $G_{13}=G_{23}=700$ MPa (calculated).

Three counterface types are used: (i) Low carbon steel St 32-7 (HB=140 N/mm², $R_e=235$ MPa, $R_m=380$ MPa), (ii) a soft zinc phosphate primer coating (alkyd-resin based, density 1.4 kg/l, 47 vol% solids) sprayed on the steel surfaces: The average coating thickness in wet conditions is 175 and 40 μm to 80 μm in dry conditions (drying time 1 h, curing time 1 week), (iii) a MoS₂ sliding spray (Gleitmo 900) with thickness 20–30 μm in dry conditions. Roughness is measured on a two-dimensional Perthen 5 SP before sliding, according to DIN 4768 and characterized by R_a (average roughness value) and R_t (peak-to-peak roughness value). The steel counterfaces have a roughness $R_a=1.12$ μm and $R_t=9.94$ μm , for zinc phosphate primer coatings is $R_a=1.29$ μm and $R_t=9.18$ μm and MoS₂ sprays have $R_a=1.05$ μm and $R_t=8.45$ μm . For good adherence of the coatings to the steel substrates, coatings were applied to sand blasted St 37-2 N with initial roughness $R_a=3.50$ μm .

2.2 Large-Scale Static Testing. Compressive loading tests on full-scale polyester/polyester B bearing elements ($\varnothing 249.50$ mm \times 40 mm) are done on a hydraulic vertical loading frame with maximum capacity of 10,000 kN. Static load tests on polyester/polyester A were not considered, as it was the main issue to investigate the stability of the lubricated top layer while the bulk properties for polyester/polyester A and polyester/polyester B are identical.

Specimens are either put "free" on a backing plate, either "constrained" in a sample holder with fixed diameter 250.00 mm and depth 32 mm, according to the boundary conditions in the practi-

Table 1 Mechanical properties for polyester/polyester composite A and B

Polyester type	Density (g/cm ³)	Tensile strength (MPa)	Compressive strength (MPa)	Elasticity modulus (MPa)	Hardness Rockwell M
A	1.25	55	365 perpendicular to fibers 95 parallel to fibers	3200	100
B	1.30	65	365 perpendicular to fibers 92 parallel to fibers		

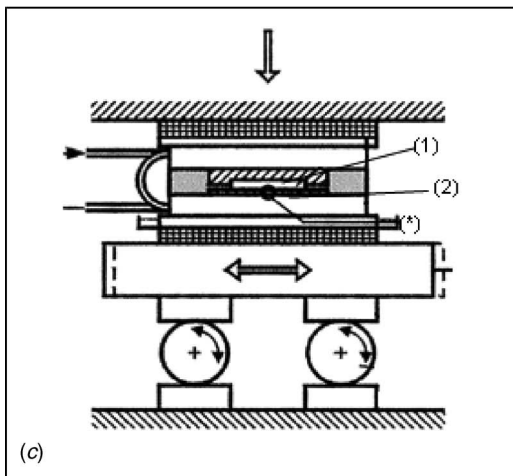
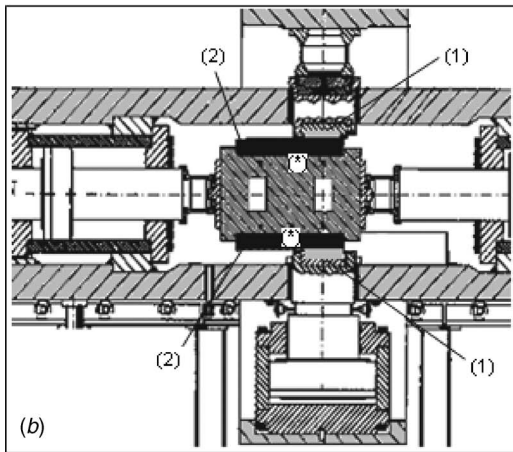
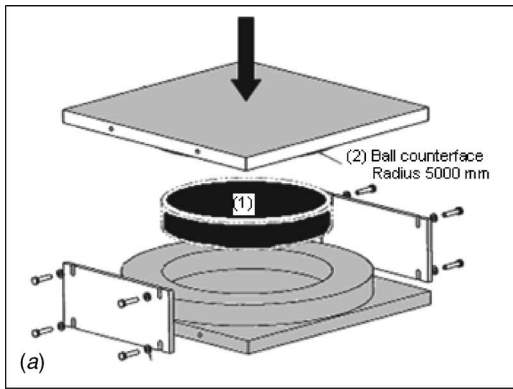


Fig. 4 Test equipment, (a) full-scale static testing (Ghent University), (b) large-scale dynamic testing (Ghent University), (c) small-scale dynamic testing (Stuttgart University) (1) composite pad, (2) counterface, (*) thermocouple

cal bearing application. A ball counterface with radius 5000 mm is used in contact with the pad top surface (Fig. 4(a)). The sample holder is horizontally centered under the hydraulic press and loaded by a vertical jack underneath, pushing the holder and its pad against the fixed upper frame plate. The vertical displacement between the upper frame plate and the table is measured by linear transducer sensors (LVDT). The contact pressure is applied at a constant rate (30 MPa/min) to a maximum of 150 MPa and then unloaded at the same rate. Intermediate contact pressures of 30, 60, 90, and 120 MPa are kept constant for 2 h during stepwise

loading, corresponding to a normal load of, respectively, 1472, 2945, 4417, 5890, and 7263 kN (72.6% of the load cell capacity). The influence of cyclic loading on stiffness and deformation is verified by subsequently applying four loading histories between 0 and 120 MPa or 0 and 150 MPa. Long-time creep is measured during a 24 h test. Recovery is measured over 24 h at stress-free conditions. Each test is done at room temperature and repeated three times, showing good reproducibility (2.4% standard deviation on the maximum indentation).

2.3 Large-Scale Dynamic Testing. Dynamic tests are done on *constrained* polyester/polyester A and polyester/polyester B composites to investigate the efficiency of the internal lubricated top layer. Two tribotesters at Ghent University (Fig. 4(b)) and Stuttgart University (Fig. 4(c)) are used, allowing to compare inter-laboratorial repeatability of the test results under identical sliding conditions: The contact pressures on each tribotester are 15, 30, 60, 90, 120, and 150 MPa at 5 mm/s sliding velocity. As the loading capacity of the test rig at Stuttgart University is limited, smaller sample diameters were applied. Pads with diameter 175 mm (scale 1:1.43) are tested on Fig. 4(b) and pads with diameter 60 mm (scale 1:4.2) or diameter 150 mm (scale 1:1.7) are tested on Fig. 4(c). Ten reciprocating sliding cycles with a single stroke of 230 mm are applied. All tests are done under atmospheric conditions (23°C, 60% relative humidity) and with the pads constrained in a sample holder with depth 32 and 8 mm free surface. Each test is repeated three times with a variation on the average friction coefficient of $\pm 5\%$.

For large-scale friction, wear and strength tests (Fig. 4(b), Ghent University), two sliding pairs are placed on top and bottom of the tribotester, each consisting of a composite pad and an uncoated or coated steel counterface (200 mm \times 410 mm). The polymer pads are fixed in circular holders in the frame of the machine, supported by leaf springs providing high stiffness to resist the horizontal sliding forces. The central sliding bloc contains two counterface plates on top and on bottom and provides a reciprocating motion through the horizontal jacks on the left (F_l) and the right (F_r). With a single sliding stroke of 240 mm, the total sliding distance comprises ten sliding cycles (one cycle is a double stroke) or 4.8 m for each normal load. The sliding velocity is fixed at 5 mm/s, controlled by a hydraulic circuit. The normal load (F_n) is applied by a jack placed in the vertical column, providing contact between the polymer test specimen and their respective steel counterfaces. Coefficients of friction are calculated according to $\mu = \frac{1}{2} |(F_l - F_r) / F_n|$ representing an average value between two friction couples. Sliding temperatures are continuously measured by a K-type thermocouple, positioned at 20 mm beneath the contact surface (i.e., at the interface of the steel counterface and the central sliding bloc). The initial counterface temperature is 15°C, obtained by internal cooling of the central sliding bloc by water flow.

Figure 4(c) (Stuttgart University) presents an alternative test rig for detailed characterization of the running-in sliding, investigating the effect of static preloads and creep on the initial static coefficient of friction and variations in friction after intermediate wear paths. The static and dynamic friction forces can be measured very accurately since the actuator is driven by a spindle and the roller bearings have very low and calibrated friction. As the maximum load capacity is lower than the Ghent University tribotester, tests are mainly performed under 15 MPa, where the highest friction is expected to occur. This is the most critical situation as literature models [25] predict lower coefficients of friction under increasing normal loads, as should be verified on the Ghent University tribotester.

3 Static Test Results

3.1 Short-Term Deformation. The compressive stress-strain characteristics for a *free* polyester/polyester B pad loaded between

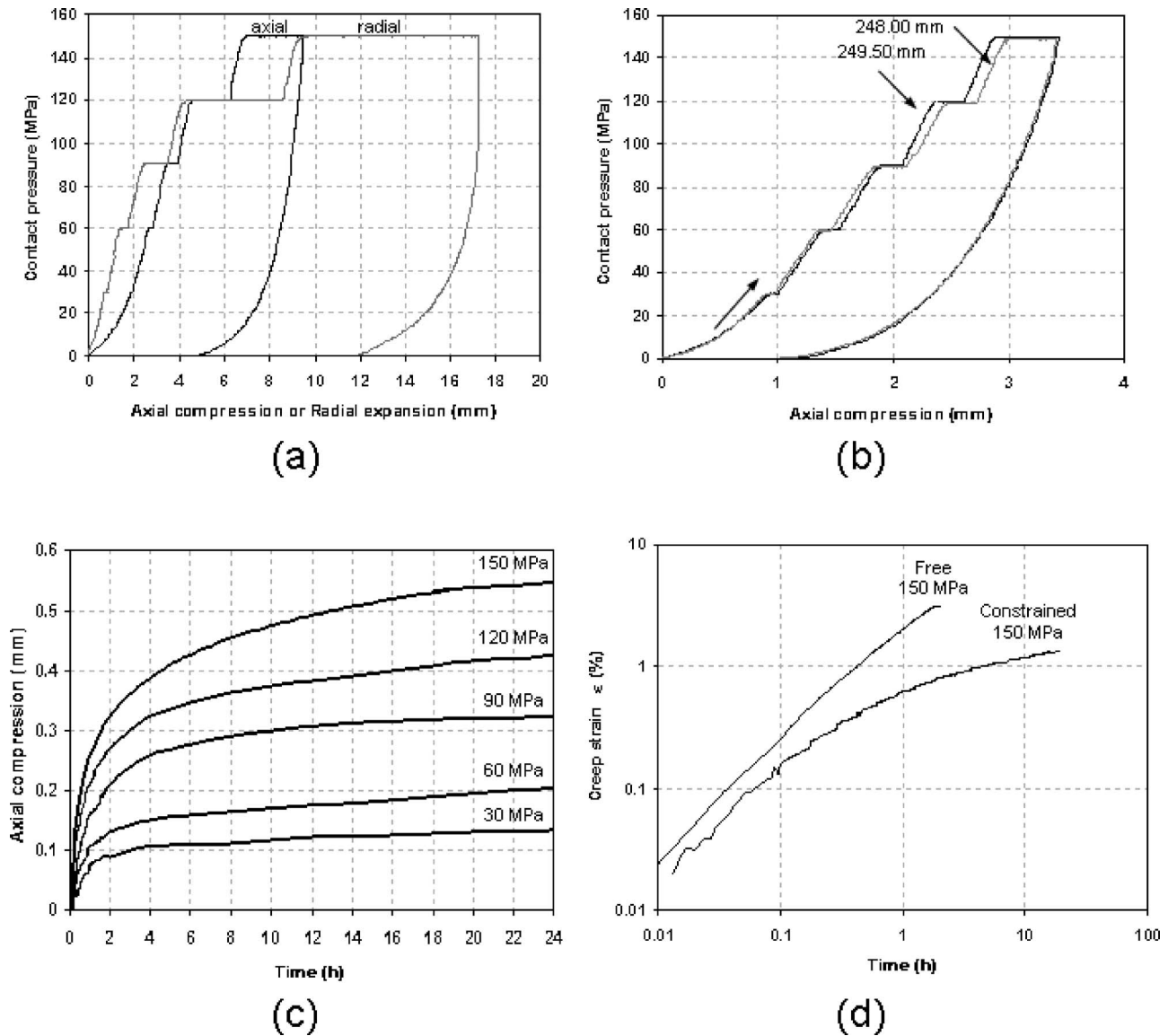


Fig. 5 Static test results for polyester/polyester B pads, (a) short-term deformation for free pads, (b) short-term deformation for constrained pads, (c) long-term deformation of constrained pads, (d) long-term deformation for free and constrained pads

0 and 150 MPa is shown in Fig. 5(a). Both the axial compression and radial expansion are plotted as a function of the contact pressure. Free composite pads show initially linear axial indentation below 10 MPa gradually changing into higher stiffness through the progressive indentation of the ball counterface and transition from initial point contact into full bearing contact. Complete contact occurs when loaded above 30 MPa and the stress-strain characteristic then has a completely linear stress-strain behavior with a constant stiffness of 2000 kN/mm over the entire contact pressure range. Important creep in both axial and radial direction occurs above 120 MPa, indicating that it is mainly a bulk phenomenon while good stability of the lubricated top layer and its interface with the composite bulk is noted at low load. The weakness of the lubricated surface layer manifests through high creep in axial compression above 120 MPa.

Figure 5(b) shows the axial compression for a *constrained* polyester/polyester B pad with a diameter of 249.50 mm or 248.00 mm fitting in a steel hole with fixed diameter of 250 mm. Samples with smaller diameter show higher axial compression due to higher clearance in the sample holder. Tolerances on the composite pads and machined steel holder are, therefore, impor-

tant for a homogeneous deformation and were studied in relation to the global deformation of the elastic bearing layer in the real ball-joint construction [22]. Constrained composite pads reveal a linear stress-strain characteristic for deformation $\epsilon < 0.01$ (or 0.20 mm axial indentation) or normal contact pressures below 10 MPa in parallel to a free composite disc, while for $\epsilon > 0.01$ or higher normal loads there is noted a gradual increase in stiffness to 4837 kN/mm at 120 MPa or 5220 kN/mm at 150 MPa. The initial similarity between free and constrained pads is attributed to a clearance of 0.50 or 1 mm between the composite pad and its holder. As soon this disappears through elastic deformation there is an increment in stiffness by the reinforcing action of the steel sample holder, causing a transition from an apparent modulus at low loads towards a bulk modulus at high loads. The increase in stiffness for constrained pads at $\epsilon > 0.01$ corresponds to a radial expansion of only 0.07 mm according to Fig. 3(a), indicating that the initial clearance has not yet totally disappeared. It is, therefore, concluded that fitting of the rubber O-ring near the bottom of the constrained pad firstly increases the stiffness through stretching, while complete radial fitting of the pad occurs when the radial

Table 2 Cyclic static deformation for a free or constrained composite pad (δ =axial compression measured at the beginning and after 2 h constant contact pressure, all values in mm)

Cycle	30 MPa		60 MPa		90 MPa		120 MPa		150 MPa		Elastic recovery	24 h recovery	Permanent deformation
	δ_1	δ_2	δ_3	δ_4	δ_5	δ_6	δ_7	δ_8	δ_9	δ_{10}			
Free polyester/polyester B pad													
Cycle 1	1.90	1.95	2.71	2.84	3.51	3.96	4.61	6.29	6.93	9.46	4.86	1.10	-2.38
Cycle 2	1.76	1.91	2.51	2.71	3.24	3.60	4.10	4.38	-	-	3.54	0.55	-2.42
Cycle 3	1.69	1.80	2.46	2.65	3.17	3.50	3.98	4.60	5.39	7.41	4.60	0.79	-2.65
Cycle 4	1.65	1.74	2.38	2.53	3.07	3.36	3.85	4.62	5.13	6.35	4.42	0.73	-3.18
Constrained polyester/polyester B pad (\varnothing 249.50 mm \times 40 mm)													
Cycle 1	1.00	1.03	1.42	1.53	1.86	2.05	2.37	2.60	2.90	3.41	2.35	0.37	-0.46
Cycle 2	1.00	-	1.42	-	1.83	-	2.25	-	2.65	-	2.32	0.36	-1.10
Constrained polyester/polyester B pad (\varnothing 174.50 mm \times 40 mm)													
Cycle 1	1.00	1.10	1.72	2.00	2.76	3.00	3.48	3.88	4.20	4.76	2.33	0.29	-0.76
Cycle 2	1.00	-	1.86	-	2.76	-	3.20	-	3.77	-	2.10	0.25	-1.22

expansion is 0.50 mm resulting in a further increase in stiffness above 20 MPa.

3.2 Cyclic Short-Term Deformation. The axial compression of a *free* polyester/polyester B pad during four loading cycles between 0 and 150 MPa with intermediate recovery over 24 h is summarized in Table 2. The permanent deformation is measured with a micrometer as the thickness reduction after recovery. The highest compression and recovery is found during the first loading cycle. For a second loading cycle only loaded to 120 MPa, the deformation is nearly completely elastic and recovered after 24 h (3.54+0.55 mm=4.09 mm compared to 4.10 mm elastic indentation). The creep during 2 h at 120 MPa is not recovered and results in an additional permanent deformation. For subsequent loading cycles, the axial compression progressively lowers with ongoing loading cycles, attributed to visco-elasticity of the composite disc. The permanent deformation of the composite pad increases after multiple loading steps.

Cyclic deformation of a *constrained* polyester/polyester B pad becomes more reproducible after multiple loading cycles. Creep during the initial loading step is favourable for reduction in clearance between the pad diameter and the sample holder diameter, eliminating influences of initial tolerances on the deformation behavior. Including a constrained composite disc with smaller dimensions (\varnothing 174.50 mm \times 40 mm) within a machined hole (\varnothing 175 mm \times 32 mm) shows higher indentation compared to full-scale tests and nonrepresentative stiffness due to the different ratio diameter/thickness compared to the full-scale tests. This justifies the full-scale testing.

3.3 Long-Term Deformation. Creep measurements for a *constrained* polyester/polyester B pad with nominal diameter 249.50 mm are given in Fig. 5(c) during 24 h loading. The total creep is between 0.10 and 0.55 mm with two regimes: a linear increase in axial deformation occurs for the 30 and 60 MPa contact pressures and there is a nonlinear creep for 90–150 MPa. In the latter cases, the axial compression linearly increases to 0.15 mm with subsequent decreasing slopes at higher loading times. According to Fig. 5(a), 0.15 mm axial compression corresponds to 0.25 mm radial expansion, as such that the initial clearance of 0.50 mm between pad diameter and sample holder has disappeared at this point.

Creep deformation is mostly described by the well-known power law verified by, e.g., Scott and Zureick [26] for time-dependent deformation of thermoplastics. The simplest form of the power law is written in Eq. (1)

$$\varepsilon(t) = \varepsilon_0 + mt^n \quad (1)$$

where $\varepsilon(t)$ =total time-dependent creep strain, ε_0 =stress-dependent and temperature-dependent initial elastic

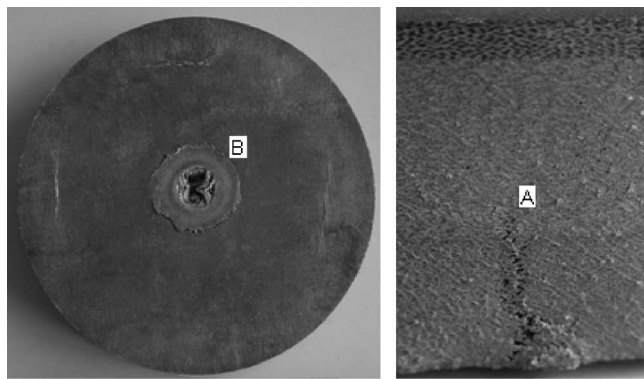
strain, t =time after loading and the parameters m and n empirical constants to be determined from a double logarithmic plot. In Fig. 5(d), creep of a free and constrained polyester/polyester pad is compared. While it is observed from the linear relation in a double logarithmic plot that free compressive deformation can be described by previous equation, the constraint of a steel sample holder causes lower deformation.

3.4 Evaluation of Overload and Failure. *Free* and *constrained* polyester/polyester B specimens after 150–200 MPa compressive tests and creep are photographed in Fig. 6. For free polyester/polyester B pads, large radial expansion of the composite bulk (“bulging”) starts at 120 MPa as also experienced on small-scale creep tests for both polyester/polyester A and polyester/polyester B by Van Paepegem et al. [24]. Vertical cracks occur over the height of the pad and the side edges remain not perpendicular to the top surface due to the free radial expansion (Fig. 6(a), A). Positioning of a free composite pad by means of a polymer screw in the real ball-joint is not possible, as a the opening for mounting the screw has failed by shear fracture above 120 MPa (Fig. 6(a), B).

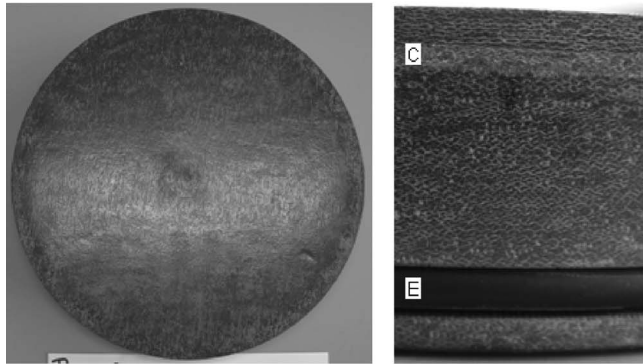
Static overload tests on constrained pads indicate a load carrying capacity to 150 MPa, while higher loads cause failure of the top surface. At low loads (60–150 MPa) there is observed a very slight radial expansion of the top surface without delamination from the composite bulk (Fig. 6(b), C). At 150–200 MPa, it shows radial expansion relatively to the composite bulk with 45 deg shear failure at the edges that are not constrained by the steel holder (Fig. 6(c), D). A surface profile of the composite pad after creep at 150 MPa and recovery indicate the permanent indentation of the convex counterface in the centre and inclined edges through shear fracture. Positioning of constrained composite pads by means of a rubber O-ring is possible, as the radial groove containing the ring has not deformed after 150 MPa contact pressures (Fig. 6(b), E). As demonstrated, the functionality of the O-ring is important for the compressive stiffness.

4 Dynamic Test Results

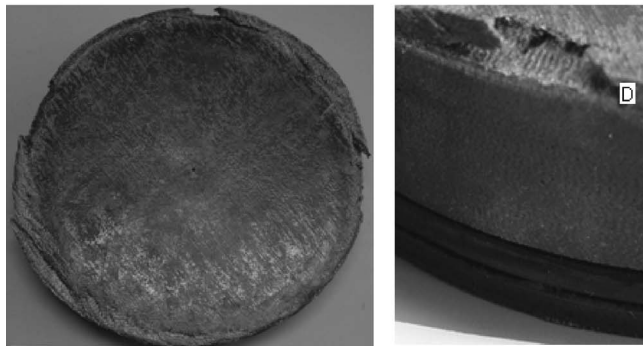
Friction curves of constrained composite pads are recorded as a function of the reciprocating sliding motion. An example of polyester/polyester B pads sliding against different counterfaces at 15 MPa is shown in Fig. 7, indicating both static and dynamic friction values during running-in. A difference is made between the values at the first sliding step (μ_{s1}, μ_{d1}) and at subsequent sliding steps (μ_{sn}, μ_{dn}).



(a)



(b)

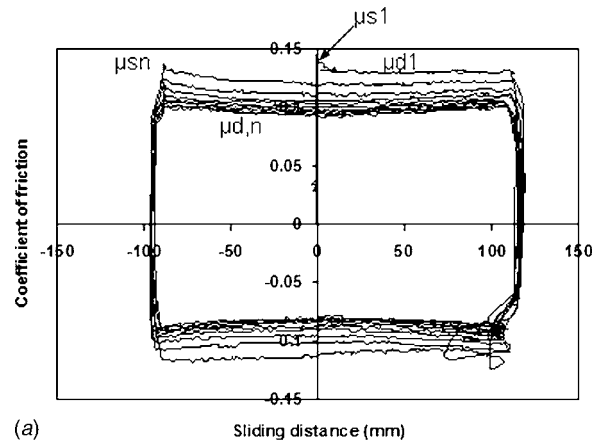


(c)

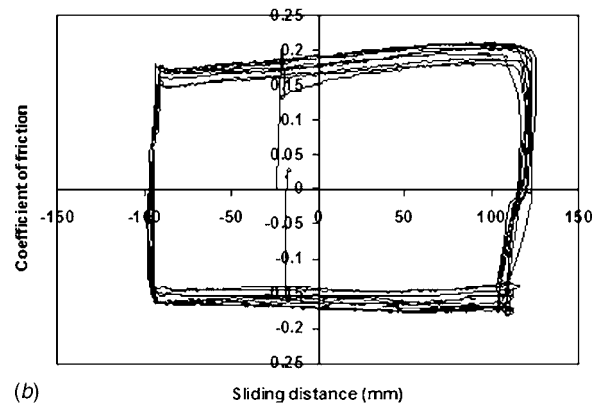
Fig. 6 Evaluation of overload and failure after static loading polyester/polyester B pads of diameter 250 mm and height 40 mm in general top view (left) and detailed side-view (right), (a) free 150 MPa, (b) constrained 150 MPa, (c) constrained 200 MPa

4.1 Effect of Composite Composition Sliding Against Steel Counterfaces.

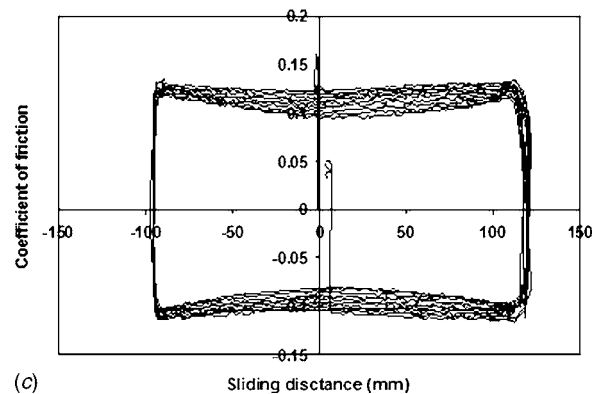
4.1.1 Friction. Table 3 gives the coefficients of friction for polyester/polyester A (pure bulk) and polyester/polyester B (with PTFE top layer) samples, sliding against a steel counterface without static preloading. The running-in behavior of polyester/polyester A is significantly detrimental at 15–60 MPa, with increasing friction as a function of increasing contact pressure, while it progressively lowers at higher contact pressures. At 15–30 MPa, also steady-state friction is unstable and increases as a function of sliding distance. Stick-slip was observed as a characteristic of unstable sliding. Polyester/polyester B shows lower and more stable friction than polyester/polyester A, except during the first sliding stroke at 15 MPa (Fig. 7(a)). As sliding then occurs against a fresh steel counterface, the lubricant in the top layer



(a)



(b)



(c)

Fig. 7 Dynamic test results for sliding of polyester/polyester B against different counterfaces at 15 MPa (running-in), (a) steel St 37-2 N, (b) MoS₂ coating, (c) zinc phosphate coating

has no influence and both static and dynamic friction coefficients are similar between polyester/polyester A and polyester/polyester B. From the second sliding stroke on, PTFE is transferred to the steel counterface, resulting in lower and more stable sliding with ongoing sliding distance. Under maximum operating conditions of 150 MPa, the friction for polyester/polyester A varies between 0.057 and 0.063 and between 0.039 and 0.042 for polyester/polyester B over three test runs, indicating that average values for both compositions in Table 3 are statistically different. This is an indication that PTFE is an effective lubricant in combination with present composite. The running-in behaviour of the polyester/polyester A or B thermosetting composite takes a longer time compared to thermoplastics as, e.g., UHMWPE [27] under identical test conditions. Establishing steady-state sliding of thermo-

Table 3 Coefficients of friction for polyester/polyester without (A) or with (B) PTFE lubricated top layer sliding against steel

p (MPa)	polyester/polyester A				polyester/polyester B			
	Running-in		Steady-state		Running-in		Steady-state	
	μ_{s1}	μ_{d1}	$\mu_{s,n}$	$\mu_{d,n}$	μ_{s1}	μ_{d1}	$\mu_{s,n}$	$\mu_{d,n}$
15	0.14	0.11	0.16	0.15	0.14	0.12	0.11	0.09
30	0.15	0.12	0.17	0.16	0.10	0.09	0.09	0.07
60	0.16	0.13	0.11	0.11	0.09	0.08	0.07	0.06
90	0.11	0.10	0.10	0.08	0.08	0.07	0.07	0.055
120	0.10	0.09	0.09	0.07	0.07	0.06	0.06	0.05
150	0.08	0.07	0.07	0.06	0.06	0.05	0.05	0.04

plastics is mainly thermally controlled and determined by plastification of the sliding surface, while the wear mechanisms for thermosetting polymers are less thermally controlled and lubricant needs to be exposed progressively from the composite bulk during steady-state sliding.

4.1.2 Sliding Temperatures. From dynamic friction and contact pressures, the bulk and flash temperatures are theoretically calculated according to models of Blok and Archard [28]. Formulas are specifically developed for circular contact geometries and compared to experimental values in Table 4. Tribological test results are considered for polyester/polyester B sliding against steel, providing lowest friction. For a uniform distribution of the heat flow over the contact area, the steady-state temperature rise at the center of the contact is given by Eq. (2) for a heat intensity $q = \mu p v$ (W/m²), contact diameter $2\ell = 175$ mm and thermal conductivity $k = 33$ W/mK. The generated heat flow is concentrated at the surface asperities of both contact bodies, resulting in a local flash temperature calculated from Eq. (3), taking into account the thermal diffusivity $a = 1.9 \cdot 10^{-4}$ m²/s.

$$T_{bulk} = \frac{q\ell}{k} = \frac{\mu p v \ell}{k} \quad (2)$$

$$T_{flash} = 1.14 \frac{\sqrt{\ell a v}}{k} \mu p \quad (3)$$

The bulk temperatures are experimentally measured at 20 mm beneath the sliding interface, and corrected by a linear conductive law with $\Delta T = qs/k = \mu p v s/k$ for a measuring depth $s = 20$ mm, estimating the bulk temperature at the sliding interface. It seems that experimental measurements of interface temperatures remain below the theoretical bulk temperatures, possibly due to convection effects not taken into account. Also complete temperature stabilisation was not attained during tests with short sliding distances (10 sliding cycles).

The calculated bulk temperatures remain below the reported maximum service temperature of 130°C, although flash temperatures may locally be higher. Thermosetting polyester/polyester

composites are not prone to softening, in contrast to thermoplastic bearing materials, but high temperatures result in local matrix degradation as discussed in Sec. 5.1.

4.1.3 Composite Wear and Deformation. Wear of the composite pads is characterised by weight measurements before and after a cumulative sliding test between 0 and 150 MPa, showing 0.85 ± 0.05 g weight loss for polyester/polyester A and 0.05 ± 0.05 g weight loss for polyester/polyester B, averaged from three test runs. A dimensional thickness reduction of -0.35 mm (measured immediately after testing) to -0.30 mm (measured one week after testing) is measured for polyester/polyester B through deformation under constrained conditions. This is lower compared to the static loading tests from Table 2 due to the shorter loading time during sliding.

The sliding surfaces of polyester/polyester A samples (Fig. 8(a)) show shear fracture near the borders perpendicular to the sliding direction at 150 MPa, characterised by crack propagation along 45 deg relatively to the top surface as a result of mechanical overload. The polyester/polyester B composite after 150 MPa sliding has a smooth surface. The lubricated top layer of 5 mm shows no delamination while it has slightly expanded in radial direction after ten subsequent sliding cycles at 150 MPa (Fig. 8(b)). For a 180 MPa overload test, the lubricated top layer has sheared relatively to the composite bulk and it is elongated parallel to the sliding direction due to delamination.

4.1.4 Polymer Transfer. The steel counterface shows no plastified polymer transfer film for polyester/polyester A, but only some separate wear debris particles that are mechanically squeezed and deposited in the roughness grooves of the steel counterface. Wear debris particles are finely dispersed at 15–120 MPa loads while they become rather scale-like at 120–150 MPa contact pressures. The wear debris particles produced at highest contact pressures look black in contrast to the original grey coloured composite material, indicating degradation. No softening and/or plastification of the thermosetting structures is possible and explains the lack of a coherent film. After removal of the transfer particles, a decrease in original steel counterface

Table 4 Evaluation of experimental and corrected bulk temperatures compared to calculated bulk and flash temperatures, according to Blok and Archard [28] (initial temperature 15°C)

Contact pressure (MPa)	Experimental bulk temperatures (°C)			Calculated temperatures (°C)	
	Measured	Correction ΔT	Interface temperature	T_{bulk}	T_{flash}
15	23	5	28	33	46
30	27	6	33	43	64
60	34	11	45	63	98
90	38	15	53	81	130
120	42	18	60	95	155
150	48	20	68	99	162

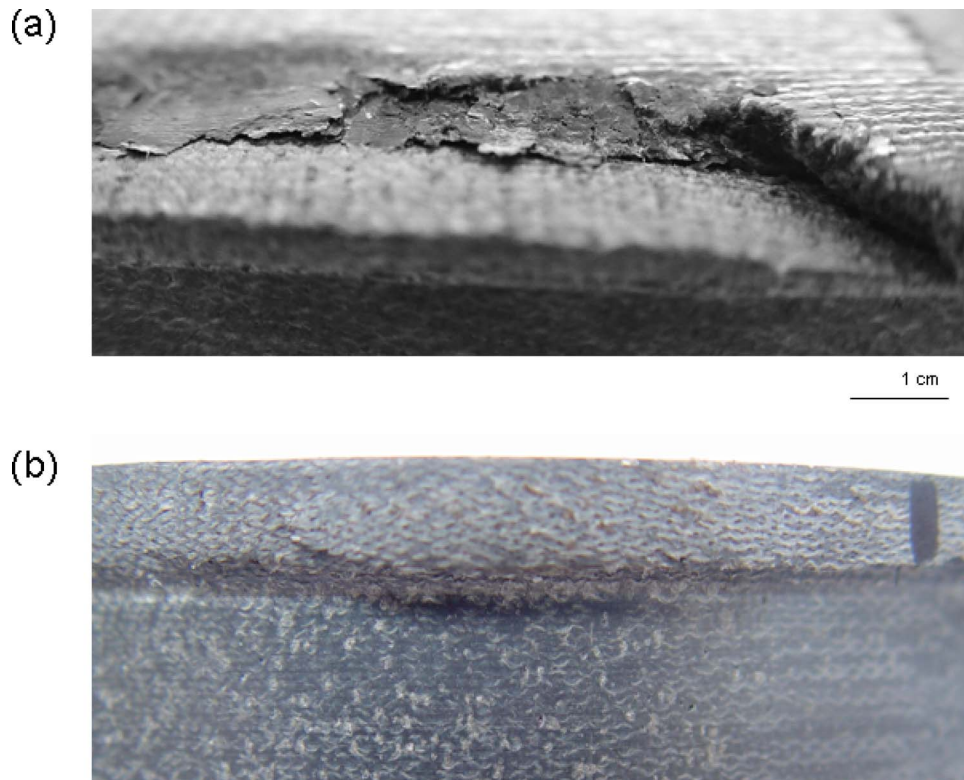


Fig. 8 Evaluation of overload and failure after dynamic sliding of composite pads of diameter 250 mm and height 40 mm, (a) polyester/polyester A at 150 MPa, (b) polyester/polyester B at 150 MPa

roughness ($R_a=1.12 \mu\text{m}$, $R_t=9.94 \mu\text{m}$) to ($R_a=1.06 \mu\text{m}$, $R_t=7.54 \mu\text{m}$) is noted, with some indications that the highest steel asperities are flattened through running-in wear of the steel counterface. For polyester/polyester B sliding against steel, a more continuous transfer film is observed being reasonably thick (Fig. 9(a)). This transfer film accords to the low and stable friction observed at 150 MPa for polyester/polyester B. The steel counterface roughness has decreased from ($R_a=1.12 \mu\text{m}$, $R_t=9.94 \mu\text{m}$) to ($R_a=0.73 \mu\text{m}$, $R_t=5.05 \mu\text{m}$) after sliding.

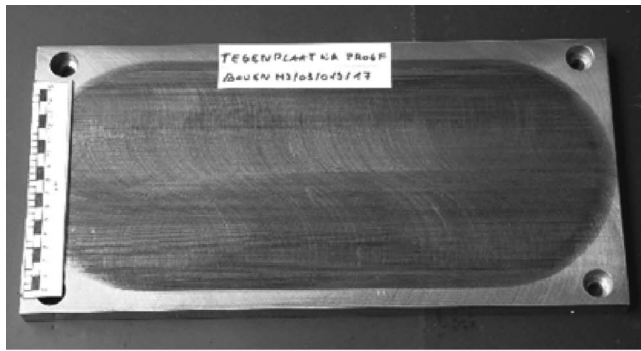
4.2 Effect of Counterface Type on Friction and Wear of Polyester/Polyester B Pads. In certain bearing design, bare steel counterfaces should be protected against corrosion by a coating. The wear and/or lubricating action of such coatings at high loads should be evaluated. For present dimensions and in situ application on the ball-joint surfaces, only a sprayed MoS_2 coating or a sprayed zinc phosphate primer coating could be considered [22]. Other two-component coatings, ceramic coatings, and metallic coatings (e.g., stainless steel, TiN, Al) could not be used due to lack of adhesion in respect to the original counterface roughness. Laboratory tests were done on the tribotester presented in Fig. 4(b) (Ghent University).

4.2.1 Friction. Coefficients of friction for polyester/polyester B pads sliding against either a MoS_2 or a zinc phosphate coating are given in Table 5. Applying a MoS_2 coating, both the static and dynamic friction coefficients significantly increase at low loads compared to bare steel surfaces. Unstable sliding with continuously increasing friction as a function of sliding distance occurs mainly at 15 MPa (Fig. 7(b)). Friction at higher contact pressures of 120–150 MPa is more stable and slightly lower on MoS_2 than on bare steel. Running-in effects with high static friction are attributed to micro structural organization of a lubricating MoS_2 coating, consisting of parallel shear layers. The original coating structure has a random orientation as the film is sprayed on the

counterface, while it progressively smoothens and orients during subsequent sliding resulting in lower friction coefficients. At higher loads and after multiple sliding steps, the woven structure of the composite sliding surface becomes impregnated by MoS_2 . A combination of PTFE solid lubricants and MoS_2 is compatible for low friction.

Also in contact with a zinc phosphate coating, high static friction is measured during the first sliding motion (Fig. 7(c)), while the friction coefficient stabilizes more rapidly compared to a MoS_2 coating. The high initial static friction compared to bare steel points to high adhesion between the polyester surface and the primer coating. For a primer coating, micro structural orientation has no influence as it was the case for MoS_2 and rather coating roughness and adhesion effects control the friction coefficient. The coating has an initial roughness $R_a=1.29 \mu\text{m}$ and $R_t=9.94 \mu\text{m}$ after spraying (which is slightly higher compared to bare steel counterfaces with $R_a=1.12 \mu\text{m}$) while it is softer compared to steel. The deformation component of friction is, therefore, increased during the first sliding strokes, reflected in a slightly higher $\mu_{d,n}$. As the coating becomes progressively smoother under sliding, the dynamic friction at high loads is lower compared to bare steel.

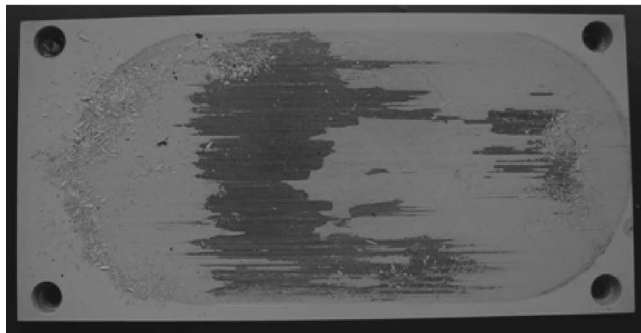
4.2.2 Coating Wear. Visual observations of the MoS_2 sliding coatings indicate progressive smoothing and degradation (Fig. 9(b)). After 15 MPa sliding, the centre of the film is thinned and slip marks occur near the borders of the sliding stroke. At 30–150 MPa the film locally detaches from the steel counterface and does not longer protect the counterface. Its roughness increases from $R_a=1.05 \mu\text{m}$ before testing to $R_a=1.46 \mu\text{m}$ after 150 MPa sliding. Coating wear does not dramatically increase the friction coefficient as it remains stable and lower compared to steel counterfaces. The detached coating substances are partially incorporated in the composite surface or remains as viscous substance in



(a)



(b)



(c)

Fig. 9 Macroscopic photograph of counterfaces after sliding with polyester/polyester B, (a) steel, (b) MoS₂ coating, (c) zinc phosphate coating

the sliding interface, acting as a lubricant. Also the zinc phosphate coating with higher coating thickness compared to MoS₂ is not compatible with polyester/polyester composites and wears. Although favorable adhesion of the coating was demonstrated during sliding against UHMWPE [27], it is partially removed after

15 MPa sliding in contact with polyester composites due to high static friction (Fig. 9(c)). As a result, coating particles are mixed with polyester/polyester wear debris particles to form a viscoelastic transfer film after multiple sliding steps. Another part of debris is removed as wear product. As the coating has thermoplastic properties, the film is continuous and smooth with consequently low friction at high contact pressures. The coating roughness decreases to $R_a=0.35 \mu\text{m}$ and $R_t=3.67 \mu\text{m}$ after sliding.

4.3 Effect of Static Preload on Friction of Polyester/Polyester B Pads. The situation of a periodic standstill of the sliding surfaces with possible creep is simulated on constrained polyester/polyester B bearing elements subjected to a static preload of 50 MPa during 16 or 48 h. The pads are therefore mounted in a backing plate with a recess of 250 mm diameter and covered with a convex counterface having no coating, a MoS₂ coating or a zinc phosphate coating. Afterwards the test specimens are transferred to the tribotester for a sliding test under different normal loads. Static and dynamic friction coefficients are summarized in Table 6, mainly at low loads as highest friction then manifests. Laboratory tests were done on the tribotester presented in Fig. 4(c) (Stuttgart University).

4.3.1 Friction. For uncoated steel counterfaces, the initial friction rises to $\mu_{s1}=0.34$ on a rough counterface ($R_a=3 \mu\text{m}$) and to $\mu_{s1}=0.22$ on a smoothed counterface ($R_a=1.12 \mu\text{m}$) after a preload of 48 h, compared to a value $\mu_{s1}=0.14$ from Table 3 without preload. The adhesive forces between the composite and steel counterfaces clearly increase and are favored through creep deformation of the composite surface, becoming microscopically compatible to the steel roughness profile. Steel surfaces with high roughness allow for higher deformation of the composite into the roughness grooves resulting in better compatibility and higher friction. The dynamic friction coefficient after preloading against uncoated steel is similar to the situation without preload (Table 3) in contrast to observations for thermoplastics, where creep possibly influences, e.g., the compaction of the crystalline structure [29]. It also indicates good reproducibility between large-scale laboratory test set-ups.

For a MoS₂ coated counterface, the initial static friction μ_{s1} has become reasonably higher than sliding tests from Table 5 without preload, exceeding the capacity of the tribotester at 10–15 MPa. As only a thin sprayed coating is applied, the roughness effect between polyester/polyester and steel still influences the contact conditions. The coating was visually damaged after the static preload. One running-in cycle could be performed at 7 MPa without overload, allowing for micro structural orientation of the lubricant film and smoothing of the sprayed coating. Elastic recovery at lower loads presumably favors lower friction. As such, the high initial friction μ_{s1} is overcome after a second sliding cycle at 15 MPa while the final dynamic friction becomes lower than obtained without preload. The latter effects are attributed to orientation of the coating, impregnation of the polyester sliding surface and subsequent controlled lubricant supply in the interface.

The friction coefficients after preload in contact with a zinc

Table 5 Coefficients of friction for polyester/polyester B sliding against coated steel

P (MPa)	MoS ₂ coating				zinc-phosphate coating			
	Running-in		Steady-state		Running-in		Steady-state	
	μ_{s1}	μ_{d1}	$\mu_{s,n}$	$\mu_{d,n}$	μ_{s1}	μ_{d1}	$\mu_{s,n}$	$\mu_{d,n}$
15	0.20	0.15	0.18	0.20	0.16	0.11	0.11	0.10
30	0.14	0.13	0.13	0.10	0.09	0.08	0.09	0.09
60	0.09	0.09	0.08	0.07	0.07	0.06	0.06	0.055
90	0.06	0.06	0.06	0.05	0.05	0.05	0.045	0.04
120	0.05	0.05	0.05	0.04	0.045	0.04	0.038	0.035
150	0.05	0.05	0.04	0.038	0.04	0.035	0.032	0.03

Table 6 Effect of a preload and roughness on large-scale friction of polyester/polyester B sliding against steel and coated steel

p (MPa)	Running-in		Steady-state		Remarks
	μ_{s1}	μ_{d1}	$\mu_{s,n}$	$\mu_{d,n}$	
Steel					
15	>0.34	-	-	-	$R_a=3 \mu\text{m}$, Overload $R_a=1.12 \mu\text{m}$
15	0.22	0.12	0.11	0.09	
MoS ₂ coating					
10	>0.55	-	-	-	Overload
12	>0.46	-	-	-	Overload
15 1° step	>0.36	-	-	-	Overload
7	0.34	0.22	0.27	0.14	Running-in
152° step	0.13	0.12	0.08	0.08	
3° step	0.09	0.09	0.08	0.08	
90	0.08	0.05	0.05	0.05	
120	0.05	0.04	0.04	0.04	
150	0.04	0.03	0.03	0.03	
Zinc-phosphate coating					
15	>0.37	-	-	-	Overload
7	>0.35	-	-	-	Overload
15	0.50	0.11	0.15	0.08	PTFE running-in spray, 48 h
15	0.26	0.06	0.06	0.06	PTFE running-in spray, 16 h
15	0.28	0.10	0.14	0.06	Grease lubricant, 48 h

phosphate counterface also indicate high initial static friction μ_{s1} and overload compared to tests without preload (Table 5). The zinc phosphate coating thickness completely masks the original steel counterface roughness and the initial contact situation is mainly controlled by adhesion. Running-in at lower contact pressures was therefore not possible, still producing overload.

4.3.2 Wear. Sliding tests against MoS₂ or zinc phosphate coatings without preload did reveal slight damage on the composite pads at 120 MPa sliding as some radial expansion of the lubricated top layer. After a static preload, the lubricated top layer of the composite pad shows stronger degradation and it is sheared relatively to the bulk composite due to high static friction. The top layer becomes elongated in the sliding direction, mainly near the sample borders as a result of stress concentrations. Internal shear fracture occurs under a 45 deg orientation.

4.4 Effect of External Lubrication. Different types of external lubricants are applied on the counterface before sliding, either a PTFE emulsion as running-in lubricant or an ultra-high pressure grease. To overcome the initial static friction in contact with a zinc phosphate coating, both lubricant types have limited success

(Table 6).

External lubricants are not very effective for reducing the static friction coefficient as they are squeezed out of the interface during initial static loading and they do not form a continuous film. Also stick-slip effects and unstable sliding remain during the first sliding cycle. In contrast, the dynamic friction coefficient during subsequent sliding cycles favorably lowers for both lubricant types as mainly attributed to progressive impregnation of the composite sliding surface by lubricant and partial release during sliding. It is observed on the polymer surfaces that the external lubricant is favorably retained into the original dry and “open” structure of the polyester fabric becoming wet. Sliding instabilities with high static friction remain at the reversals of the sliding motion due to a periodic standstill and interferences between slight elastic kick-back and lubricant supply.

5 Discussion

5.1 Composite Wear and Failure Mechanisms. The sliding surface of the original composite structure for polyester/polyester B is shown in Fig. 10(a) with lubricating PTFE. A detail of the

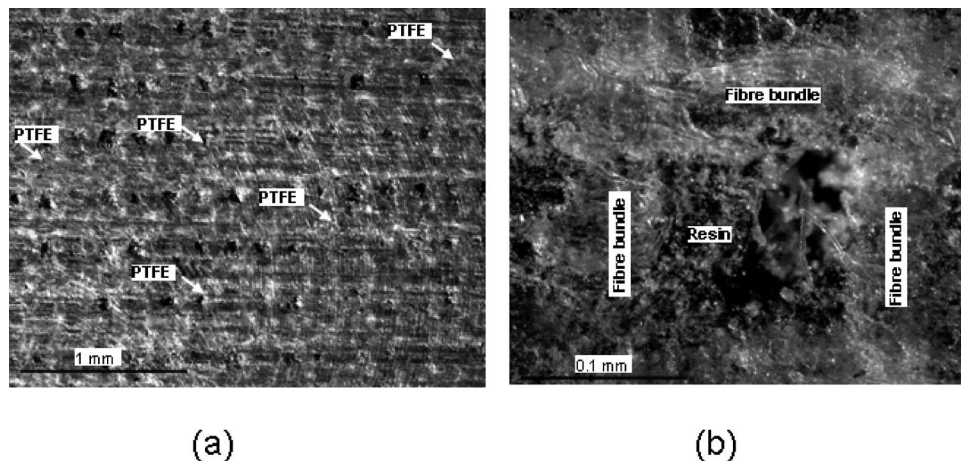


Fig. 10 Original polyester/polyester B structure, (a) overview with distribution of PTFE, (b) detail of impregnated fiber fabric

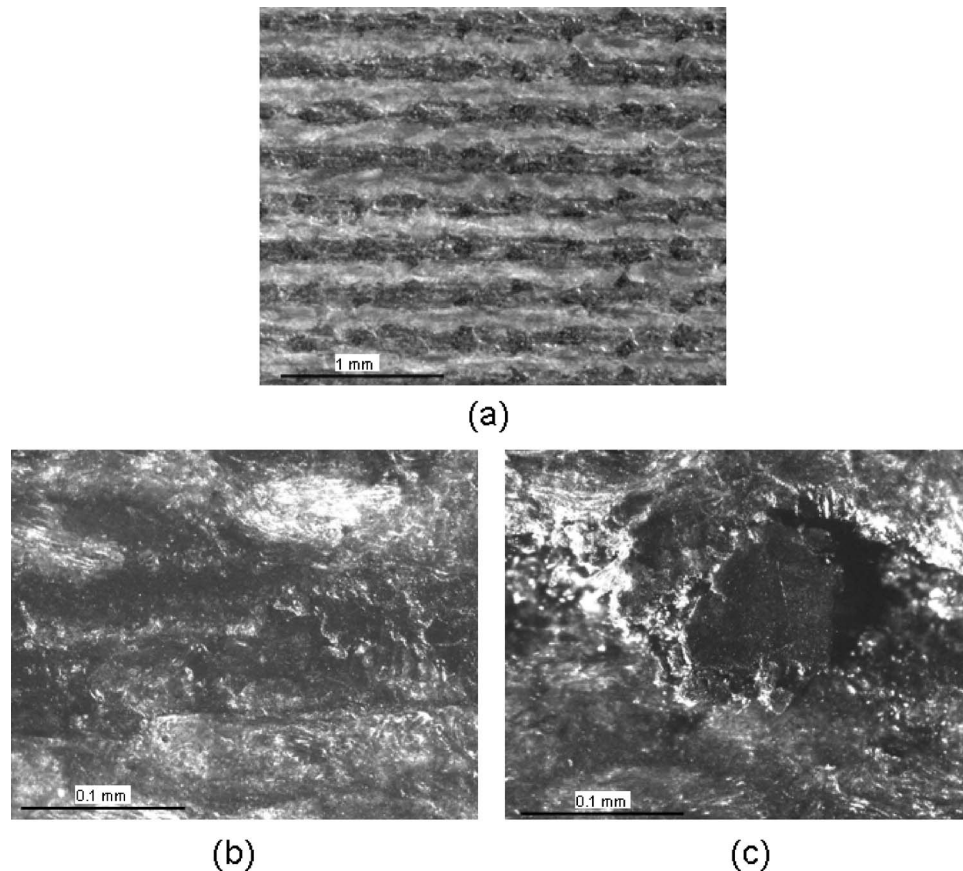


Fig. 11 Matrix wear mechanisms for polyester/polyester A characterized by matrix removal and lack of sliding film formation, (a) matrix removal and fiber exposure, (b) matrix shear, (c) removal of degraded particles

fabric (Fig. 10(b)) shows bundles of polyester fibers with some of them free exposed to the surface. No additional surface layer is added. The woven polyester structure is impregnated by the matrix with good adhesion between the matrix and the fiber, while voids are observed in between the fabric.

5.1.1 Matrix Wear. After sliding tests under mild conditions, most significant wear features occur in the matrix rather than the fabric reinforcement, as it has lowest wear resistance. The observed wear types of the thermosetting polyester matrix are detailed in Fig. 11. Polyester/polyester A surfaces indicate that the matrix is removed parallel to the sliding direction and the fiber structure becomes more visible (Fig. 11(a)). Local black spots show that the polyester has thermally degraded (carbonization) and fractures. Surface pits in the composite matrix are, therefore, observed by either tearing of wear debris particles (low loads) or brittle fracture (high loads) from the composite matrix. A detail of a shear zone in the polyester matrix is observed on a detail in Fig. 11(b) and a detail of a polyester particle removed from the matrix is shown in Fig. 11(c). This is expected due to the progressive transition into a brittle nature of polyesters at higher temperatures [14], which get fractured due to high external stress rather than plastic deformation. After the particles are removed from the matrix they are transported towards the centers of the sliding stroke. Wear debris of polyester/polyester A is separately found near the borders of the sliding stroke. The observation of small particles at low loads and large particles at higher loads is in accordance with present matrix degradation through brittleness.

With added PTFE in polyester/polyester B, a continuous sliding film develops on top of the matrix and fibers while no separate wear debris particles are observed. As PTFE is a thermoplastic lubricant, it plasticizes favorably and establishes a film incorpo-

rating the degraded polyester wear debris particles (Fig. 12(a)). At low loads, the film is rather thin and only observed between the fiber bundles while it becomes progressively thicker and covers the entire sliding surface at high loads. This is attributed to the progressive wear and release of PTFE from the composite bulk at higher loads. In the latter case, the brittle fracture of the polyester constituent of the film prevails and particles are removed from the film (Fig. 12(b)). Also the increased thickness of the film makes it more brittle and fracture is located on top of the fibers due to stress concentrations.

5.1.2 Fiber Wear. Fiber wear induced by dynamic loads is only observed for polyester/polyester A. The fibers are directly sheared and not protected by a sliding film after the matrix is removed, resulting in local pull-out of some fibers (Fig. 13(a)). Some scarce fiber fracture is observed near the borders of the test sample due to a combination with static overload (Fig. 13(b)). The fibers are protected by a sliding film at high loads and show no shear related failure up to 150 MPa for polyester/polyester B.

5.1.3 Overload Failure. More severe fiber wear is noted near the borders of the test specimens for both polyester/polyester A and polyester/polyester B after static or dynamic loading at 150 MPa. Interlaminar shear failure (Fig. 14(a)) and matrix debonding (Fig. 14(b)) are due to overload under both static and dynamic loading and indicate that static overload is the main cause for catastrophic failure. Under dynamic loading, interlaminar shear is observed at the borders perpendicular to the sliding direction and matrix debonding mainly occurs at the borders parallel to the sliding direction. Also significant is that these failure types occur for both polyester/polyester A and polyester/polyester B composites, indicating that they are clear bulk failure mecha-

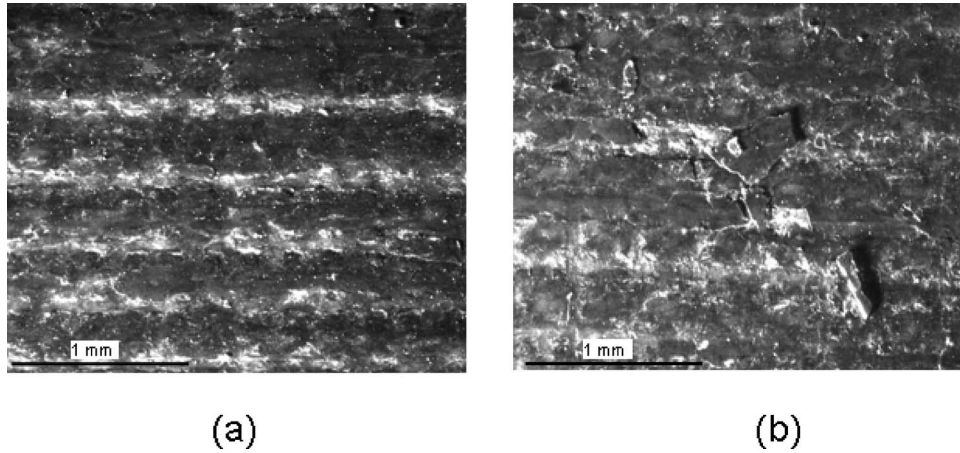


Fig. 12 Matrix wear mechanisms for polyester/polyester B characterized by sliding film formation, (a) film covering matrix phase, (b) film covering both matrix and fiber phases with fracture through brittleness at high loads

nisms not depending on eventual weakness of the PTFE lubricated top layer. A detail on the fibers in the shear zones shows fiber-pull out rather than fiber fracture (Fig. 14(c)). It indicates that the overload failure mechanism is ductile rather than brittle and after fracture of bulk fragments through shear, it is not readily detached from the composite pad being free circulating in the sliding interface.

5.2 Counterface Wear Mechanisms. An optical micrograph of the steel surfaces is shown in Fig. 15, with depositions of some degraded wear debris for polyester/polyester A and the formation of a continuous transfer films for polyester/polyester B. In the latter case, plastification of thermoplastic PTFE is clearly noted incorporating thermosetting wear debris particles. At high loads, the film becomes brittle and is only deposited in the roughness grooves.

Both the MoS₂ and zinc phosphate coatings are worn through adhesive wear. Adhesion between the respective coatings and the composite sliding surface is illustrated in Figs. 16(a) and 16(b). The voids in the composite structure are effective in absorption of a MoS₂ sliding spray, forming a continuous sliding film on the composite surface. A similar behavior is noticed after application of external lubricant as, e.g., grease. The bulk composite structure is, therefore, protected against wear. A strong adhesion between zinc phosphate fragments and the polyester bulk possibly establishes through the thermoplastic properties and plastic deformation of coating fragments. Chemical reactions during sliding may

also contribute to the formation of adhesive bonds between the coating and polyester sliding surface, possibly leading to the formation of, e.g., zinc-stearates that have beneficial lubricating ability as shown by Bahadur et al. [9].

Although MoS₂ and zinc phosphate are effective lubricants for low friction at high loads, they are easily removed from the counterface as shown in Figs. 16(c) and 16(d). Mainly near the reversals of the sliding stroke, stick-slip lines are observed in the MoS₂ film where the steel surface becomes visible. The zinc phosphate shows better adhesion to the steel counterface, as no interfacial delamination is observed. The steel surface remains covered by a thin lubricating film with incorporation of polyester/polyester wear debris.

6 Conclusions

Friction, wear mechanisms and overload failure of polymer composites made of a thermoplastic polyester fiber fabric impregnated by a thermosetting polyester resin were evaluated on large-scale test equipment. It is concluded that:

- (1) The material shows complete elastic recovery after short-time loading to 120 MPa. Creep at 120 MPa results in permanent deformation. Constrained elements have a load bearing capacity to 180 MPa, while overload at 200 MPa is characterized by interlaminar shear failure near the sample edges.

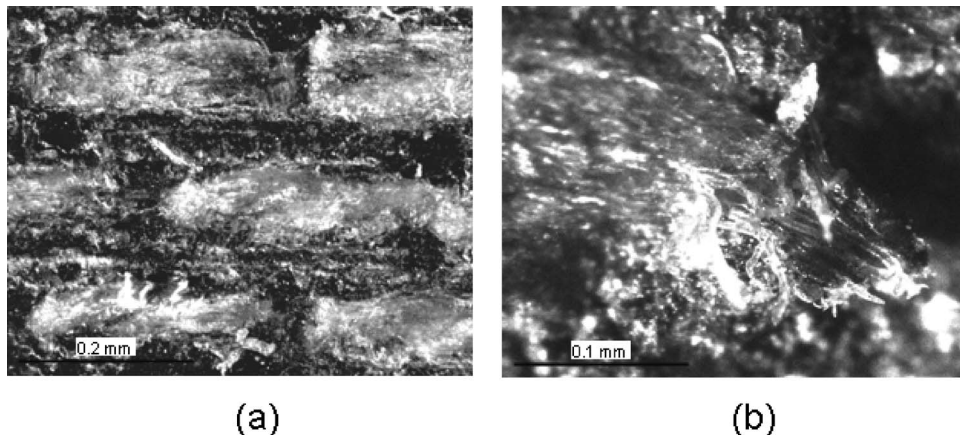
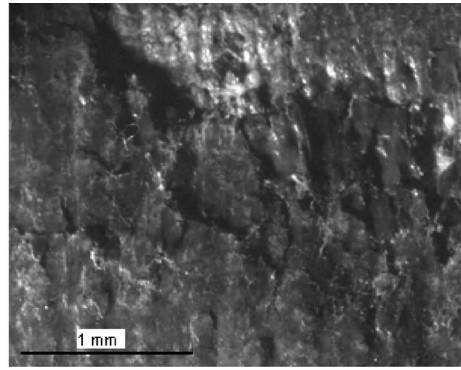
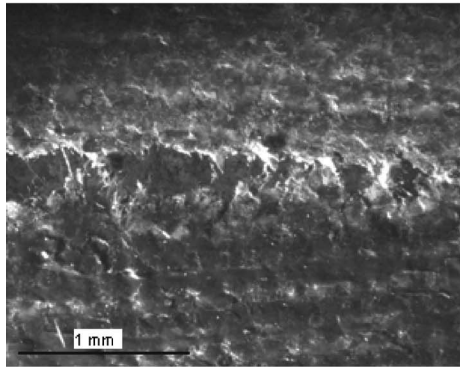


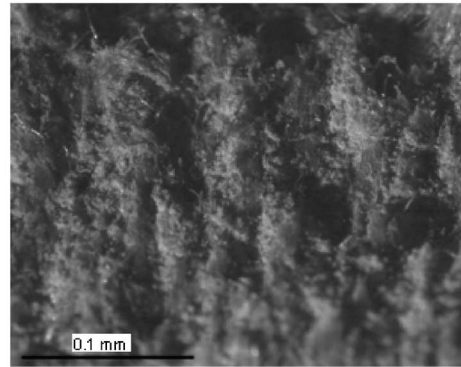
Fig. 13 Fiber wear mechanisms for polyester/polyester A, (a) fiber pull-out, (b) fiber fracture



(a)



(b)



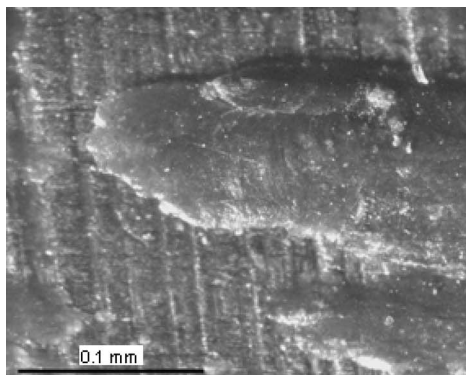
(c)

Fig. 14 Overload failure mechanisms for polyester/polyester A and B, (a) interlaminar shear failure, (b) debonding, (c) fiber pull-out

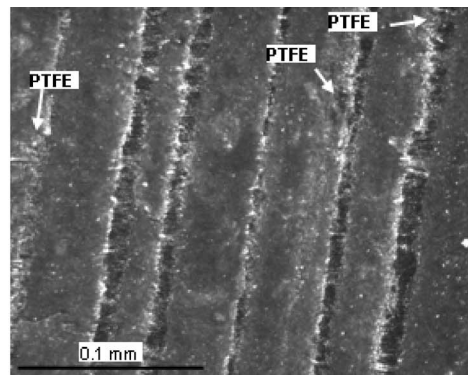
(2) Dynamic overload occurs at 150 MPa due to expansion of the nonconstrained top surface and overload at 180 MPa due to interlaminar shear failure. After preliminary creep deformation, the nonconstrained top surface becomes dimensionally unstable when slid above 120 MPa and overload occurs at 150 MPa. The constrained composite bulk behaves under hydrostatic stress conditions that lack at the sliding surface. An effective stress of 92 MPa near the edges of the test samples then causes failure.

(3) A MoS₂ coating favorably reduces friction at high loads, while it shows unstable running-in features at low loads possibly related to the molecular structure that progressively orients during sliding. The composite surface becomes impregnated by the lubricating film and, therefore, shows high adhesion and static friction after preliminary creep. The adhesion of the coating to the steel surface is inferior and causes removal after a short sliding time.

(4) A zinc phosphate primer coating also adheres strongly



(a)



(b)

Fig. 15 Steel counterfaces after sliding, (a) separate wear debris transfer for polyester/polyester A, (b) transfer film formation for polyester/polyester B

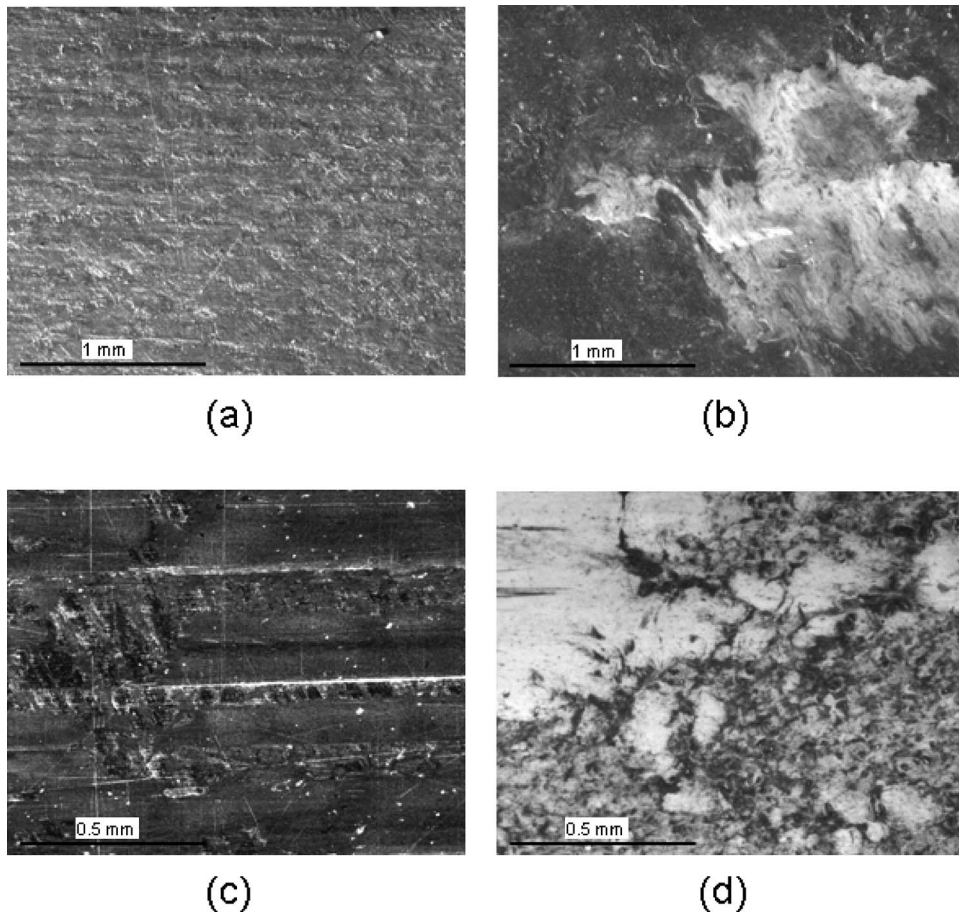


Fig. 16 Coating adhesion and removal, (a) polyester/polyester B surface impregnated by MoS₂, (b) polyester/polyester B surface with adhesion of zinc-phosphate, (c) removal of MoS₂ on the steel surface, (d) wear of zinc phosphate on the steel surface

to the composite surface, resulting in high static friction and coating removal. The coating wears partially through internal delamination but still adheres to the steel counterface. A thin lubricating film with mixed thermoplastic coating particles and thermosetting polyester/polyester composite particles establishes and causes low friction at high contact pressures.

- (5) PTFE lubricants are compatible with the thermosetting bulk composite, providing a continuous film on steel counterfaces.
- (6) Wear mechanisms are mainly governed by thermal matrix degradation at maximum flash temperatures of 162°C, resulting in shear fracture at low loads and brittleness at higher loads. For PTFE-filled polyesters, a continuous film develops on the composite surface protecting against fiber wear. Evidence of fiber pull-out and fiber fracture is noted after sliding of nonlubricated composite and after static overload.

Acknowledgment

The authors express their gratitude to the Ministry of Transport, Public Works and Water Management (The Netherlands) and Solico B.V., allowing to present the test results and to be involved in the redesign of the Maeslant storm surge barrier.

References

- [1] Hollaway, L. C., 1990, *Polymers and Polymer Composites in Construction*, Thomas Telford, London.
- [2] Scott, D. H., 1992, *Materials for Friction and Wear Applications*, ASM Hand-

book, ASM International, Materials Park, PA, Vol. 18, p. 820.

- [3] Zsidai, L., De Baets, P., Samyn, P., Kalacska, G., Van Peteghem, A. P., and Van Parys, F., 2002, "The Tribological Behavior of Engineering Plastics During Sliding Friction Investigated With Small-scale Specimens," *Wear*, **253**, pp. 637–688.
- [4] Bijwe, J., Indumathi, J., Rajesh, J., and Fahim, M., 2001, "Friction and Wear Behavior of Polyetherimide Composites in Various Wear Modes," *Wear*, **249**, pp. 715–726.
- [5] Naga, S. A. R., 1992, "Wear Behavior of Glass Reinforced Polyamide 66," in *Proc. of 5th International Conference on Applied Mechanical Engineering*, Cairo, Egypt, pp. 157–162.
- [6] Kishore, Sampathkumaran, P., Seetharamu, S., Murali, A., and Kumar, R. K., 2001, "On the SEM Features of Glass-Epoxy Composite System Subjected to Dry Sliding Wear," *Wear*, **247**, pp. 208–213.
- [7] Srivasstava, V. K., Pathak, J. P., and Tahzibi, K., 1992, "Wear and Friction Characteristics of Mica Filled Fibre Reinforced Epoxy Resin Composites," *Wear*, **152**, pp. 343–350.
- [8] Jacobs, O., Jaskulka, R., Yang, F., and Wu, W., 2004, "Sliding Wear of Epoxy Compounds Against Different Counterparts Under Dry and Aqueous Conditions," *Wear*, **256**, pp. 9–15.
- [9] Bahadur, S., Zhang, L., and Anderegg, J. W., 1997, "The Effect of Zinc and Copper Oxides and Other Zinc Compounds as Fillers on the Tribological Behavior of Thermosetting Polyester," *Wear*, **203-204**, pp. 464–473.
- [10] Friedrich, K., and Reinicke, P., 1998, "Friction and Wear of Composite Materials," *Mech. Compos. Mater.*, **34**, pp. 503–514.
- [11] Chand, N., and Neogi, S., 2002, "Sliding Wear Behavior of Woven Glass Fiber Reinforced Polyester Composites," *Ind. J. Eng. Mater. Sci.*, **9**, pp. 299–306.
- [12] Vishwanath, B., Verma, A. P., and Rao, C., 1993, "Effect of Different Matrices on Wear Characteristics of Glass Woven Roving Polymer Composites," *Composites*, **24**, pp. 347–353.
- [13] Bahadur, S., and Zheng, Y., 1990, "Mechanical and Tribological Behavior of Polyester Reinforced With Short Glass Fiber," *Wear*, **137**, pp. 251–266.
- [14] Pihili, H., and Tosun, N., 2002, "Investigation of the Wear Behavior of a Glass-Fiber-Reinforced Composite and Plain Polyester Resin," *Int. J. Compos. Sci. Technol.*, **62**, pp. 367–370.
- [15] El-Tayeb, N. S., and Mostafa, I. M., 1996, "The Effect of Laminate Orientations on Friction and Wear Mechanisms of Glass Reinforced Polyester Com-

- posite,” *Wear*, **195**, pp. 186–191.
- [16] Tsukizoe, T., and Ohmae, N., 1983, “Friction and Wear of Advanced Composite Materials,” *Wear*, **200**, pp. 95–104.
- [17] Chand, N., Naik, A., and Neogi, S., 2000, “Three-Body Abrasive Wear of Short Glass Fiber Polyester Composite,” *Wear*, **242**, pp. 38–46.
- [18] Zhang, Z., Breidt, C., Chang, L., Hauptert, F., and Friedrich, K., 1994, “Enhancement of the Wear Resistance of Epoxy: Short Carbon Fibre, Graphite, PTFE and Nano-TiO₂,” *Composites, Part A*, **35**, pp. 1385–1392.
- [19] Theiler, G., Hübner, W., Gradt, T., Klein, P., and Friedrich, K., 2002, “Friction and Wear of PTFE Composites at Cryogenic Temperatures,” *Tribol. Int.*, **25**, pp. 449–458.
- [20] Quintelier, J., Samyn, P., Van Paepegem, W., De Baets, P., Vermeulen, J., Tuzolana, T., and Van den Abeele, F., 2006, “Wear Behavior of Carbon Fiber Reinforced Poly-Phenylene Sulfide,” *Polym. Compos.*, **27**, pp. 92–98.
- [21] Leendertz, J. S., Van Schepdael, L., Van Paepegem, W., Samyn, P., De Baets, P., and Degrieck, J., 2006, “Änderungen Der Gelenklagerkonstruktion Des Sturmflutsperrwerks Bei Rotterdam,” *Stahlbau*, **75**, pp. 45–54.
- [22] Samyn, P., Leendertz, J. S., Suister, E., Van Schepdael, L., Van Paepegem, W., Degrieck, J., and De Baets, P., “Global Analysis and Constructional Aspects in the Redesign of Bearing Elements for a Movable Storm Surge Barrier,” *Eng. Struct.* (to be published).
- [23] Busak, and Shamban, 1998, “Luytex–Composite Materials,” company brochure.
- [24] Van Paepegem, W., Van Schepdael, L., Degrieck, J., Samyn, P., De Baets, P., Suister, E., and Leendertz, J. S., “Fast Characterization of Carbon/Epoxy Rings for Use in the Ball-Joints of the Maeslant Storm Surge Barrier,” *Compos. Struct.* (to be published).
- [25] Yamaguchi, Y., 1990, *Tribology of Plastic Materials*, Tribology Series 16, Elsevier, Amsterdam.
- [26] Scott, D. W., and Zureick, A. H., 1998, “Compression Creep of Pultruded E-Glass/Vinylester Composite,” *Compos. Sci. Technol.*, **58**, pp. 1361–1369.
- [27] Samyn, P., Van Schepdael, L., Leendertz, J. S., Gerber, A., Van Paepegem, W., De Baets, P., and Degrieck, J., 2006, “Large-Scale Friction and Wear Tests on a Hybrid UHMWPE-Pad / Primer Coating Combination Used as Bearing Element in an Extremely High-Loaded Ball-Joint,” *Tribol. Int.*, **39**, pp. 796–811.
- [28] Dunaevsky, V. V., and Booser, E. R., eds., 1997, *Tribology Data Handbook*, CRC Press, New York, p. 462.
- [29] Lee, K. Y., and Pienkowski, D., 1997, “Reduction in the Initial Wear of UHMWPE After Compressive Creep Deformation,” *Wear*, **203–204**, pp. 375–379.